TURBULENCE STRUCTURE, FRICTION DRAG AND PRESSURE DRAG DUE TO TURBULENT FLOW OVER ANGLED WAVY SURFACES

Hideto Fujii
Department of Mechanical and System Engineering
Kyoto Institute of Technology
Matsugasaki, Sakyo-ku, Kyoto 606-8585, Japan
m0623039@edu.kit.ac.jp

Katsutoshi Sakurai
Department of Mechanical and System Engineering
Kyoto Institute of Technology
Matsugasaki, Sakyo-ku, Kyoto 606-8585, Japan

Tadashi Nakano
Department of Mechanical and System Engineering
Kyoto Institute of Technology
Matsugasaki, Sakyo-ku, Kyoto 606-8585, Japan

Yoshimichi Hagiwara
Department of Mechanical and System Engineering
Kyoto Institute of Technology
Matsugasaki, Sakyo-ku, Kyoto 606-8585, Japan
yoshi@kit.ac.jp

ABSTRACT

We carried out direct numerical simulation for turbulent flow over angled wavy walls. The walls are models of the folded areas of skin which appear on the abdominal parts of fast swimming dolphins. The angles between the streamwise direction and the ridgelines of the wavy walls were 90, 63.4 and 45 degrees. The ratio of amplitude to wavelength in the streamwise direction of the wavy wall was 0.0064. The computational results show that the mean velocity in the transverse direction becomes predominant as the angle decreases. This is due to the occurrence of secondary flow along the ridgelines of the wavy walls. It is also found that the wall-shear stress tensor decreases with the decrease in the angle. This is because the contribution of the Reynolds-shear-stress component $-\rho\overline{u'w'}$ becomes more noticeable with the decrease in the angle. The local modification of coherent structure caused by the secondary flow along the ridgelines leads to the decrease in the Reynolds shear stress.

INTRODUCTION

The reduction of drag acting on a moving body in fluid has been focused on for many years in various research fields. The reduction of drag acting on swimming dolphins is not an exception. Several possible mechanisms have been discussed for this drag-reduction. These include (1) viscous damping by compliant skin, (2) an induced turbulent boundary layer and (3) boundary layer acceleration (Fish, 2006). Folds of skin are another possible mechanism. If a folded skin is regarded as a two-dimensional rigid wavy surface, the skin is not advantageous for drag reduction: the pressure drag increases noticeably with the ratio of amplitude to wavelength of the wavy surface (Henn and Sykes, 1999), while the friction drag decreases slightly with an increase in the ratio (Tuan et al., 2006). Thus, the total drag increases noticeably with the ratio (Nakagawa and Hanratty 2003).

The research group of present authors has focused on the differences between the two-dimensional rigid wavy sinusoidal surfaces and dolphin skins. One of the differences is the angle of the ridgelines of the folds. The ridgelines observed are not perpendicular to the body axis of the swimming dolphins, and thus to the main-flow direction (Zhang et al., 2007). In our previous experiments (Yoshitake et al., 2008, Ozaki et al., 2009), we measured the total drag and the friction drag for small angled wavy plates on the bottom of an open channel. In these experiments, the increase in the total drag was lower than expected. This is because the

recirculation flow, which occurs near the trough of the wavy surface, is intermittent. However, due to limitation of measurement, the effects of the angle on the friction drag and total drag have not yet been examined.

In the present study, we carry out direct numerical simulation for turbulent flow over angled wavy surfaces to elucidate the effects of the angles of the ridgelines on the two kinds of drags and the local turbulence structure.

COMPUTATIONAL METHOD

Assumptions

We made the following assumptions:

(1) The wavy walls are stationary. However, the folded skins of dolphins may move due to the shear force.
(2) The ridgelines of the wavy walls are parallel.
(3) The surfaces of the wavy walls are smooth. The slightly rough texture of actual dolphin skins has not been taken into account.

Computational domains

We dealt with turbulent flow in a domain between an upper shear-free lid and a lower non-slip deformed wall as shown in Fig. 1. The method for the formation of the wavy wall is described later. The *x*-, *y*- and *z*-axes were positioned in the streamwise, vertical and transverse directions, respectively. The ξ- and η-axes were positioned along the wall and the wall-normal direction, respectively. The domain was converted to the computational domain, which was a rectangular box of $2\pi h \times h \times 2\pi h$, by using an unsteady generalized curvilinear coordinate system to fit the deformed wall at any moment.

Schemes and grid arrangement

The Navier-Stokes equations were discretized with a staggered grid system. The grid spacing was identical both in the ξ- and *z*-directions. The spacing increased from the lower and upper walls in the η direction based on a hyperbolic tangent. The grid resolution was $\Delta x^+ = 14.7$, $\Delta y^+ = 0.394 - 4.75$ and $\Delta z^+ = 7.36$ in the case of flat wall. (The grid resolution $\Delta\xi^+$ is slightly longer than Δx^+, while $\Delta\eta^+$ is slightly longer or shorter than Δy^+ depending on the location.) The time increment was $\Delta t^+ = 0.02$. The computational schemes were the same as those used by Koyama et al. (2007). The details are shown in Table 1.

Boundary and initial conditions

The periodic boundary condition was applied for velocity and pressure in the ξ- and *z*-directions. A non-slip boundary condition was adopted for the lower deformed wall, while a free-slip boundary condition was adopted for the upper imaginary wall. A database made up of fully developed flow over a flat wall was adopted as the initial velocity field.

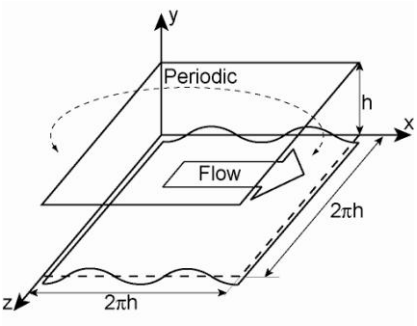

Figure 1. Computational domain.

Table 1 Computational condition.

Grid	Collocated Grid
Grid number	64×64×128
Grid resolution	
Δx^+ (= $\Delta x\, u_\tau / \nu$)	14.7
Δy^+ (= $\Delta y\, u_\tau / \nu$)	0.394-4.75
Δz^+ (= $\Delta z\, u_\tau / \nu$)	7.36
Coupling Algorithm	Fractional Step Method (FFT&Residual Cutting Method)
Reynolds number Re_τ (= $u_\tau h / \nu$)	150
Time evolution scheme	3rd-order accurate *Runge-Kutta* scheme
Boundary condition	
x,z-direction	Periodic
y-direction	Upper: slip Bottom: non-slip
Difference scheme	4th-order central difference

Computational conditions

The Reynolds number was $Re = hu_\tau/\nu = 150$ where ν is the kinematic viscosity and u_τ is the friction velocity at the initial state. Table 2 shows the conditions of the amplitude and angles. The amplitude of the wavy wall A_{max} was set equal to $3\nu/u_\tau$. The flat wall is referred to as case 1. The angles between the *x*-axis and the ridgelines γ were 90 degrees, perpendicular to the main flow (case 2), 63.4 degrees (case 3) and 45 degrees (case 4). Figure 2 shows the wavy surface in case 3.

Generation of angled wavy walls

In the period of $0 < t < T_{wd}$ for the preliminary computation, we increased the amplitude of the wavy walls by using the following equation:

$$A(t) = A_{max} \sin \frac{2\pi t}{T_{wd}}, \quad (1)$$

Table 2 Conditions of amplitude and angle.

	case1	case2	case3	case4
A^+_{max}	0	3	3	3
γ	–	90	63.4	45

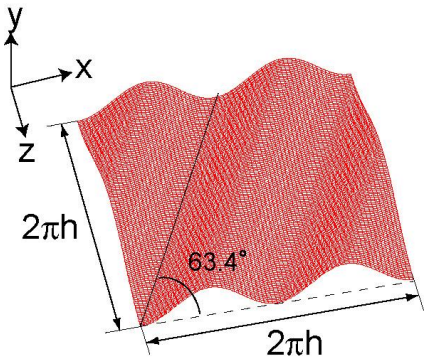

Figure 2. Computational mesh on the bottom wall(γ=63.4°).

where t is time and T_{wd} is the period of deformation. T_{wd}^+ was 30. The local, instantaneous height of the wall y_w can be expressed by the following equation:

$$y_w(x,z,t) = -A(t)\cos\frac{4\pi}{L_x}\{x + z\tan(\pi-\gamma)\}. \quad (2)$$

In this equation, the angles between the streamwise direction and the ridgelines of the wavy walls are given by the following equations in cases 3 and 4:

$$\text{In case 3}, \gamma = \tan^{-1}\frac{2L_z}{L_x}, \quad \text{In case 4}, \gamma = \tan^{-1}\frac{L_z}{L_x}, \quad (3)$$

where L_x and L_z are the dimensions of the computational domain in the x- and z-directions respectively.

After T_{wd}, the amplitude was unchanged at A_{max}. Thus, the local height of the wall is expressed as follows:

$$y_w(x,z,t) = -A_{max}\cos\frac{4\pi}{L_x}\{x + z\tan(\pi-\gamma)\}. \quad (4)$$

RESULTS AND DISCUSSION

In order to make the discussion clear, we divided the wavy walls and the space above the wall into the following six sub surfaces and sub-spaces as shown in Fig. 3: valley, uphill1, uphill2, hilltop, downhill2 and downhill1.

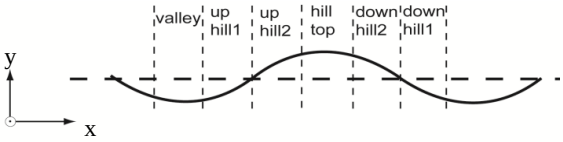

Figure 3. Classification of regions above wavy wall.

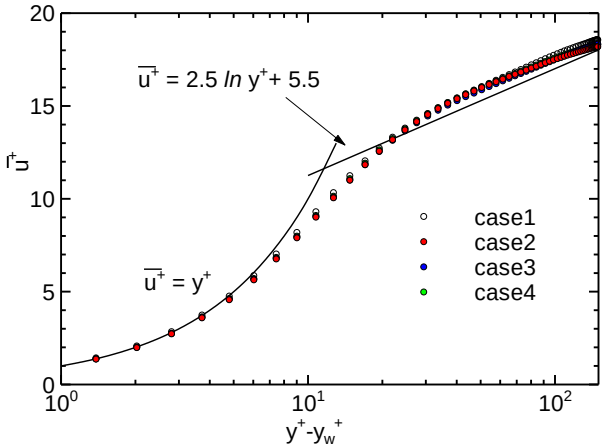

Figure 4. Mean velocity in the streamwise direction.

Mean velocities

Figure 4 indicates the mean velocity profiles in the streamwise direction. The mean velocity in the inner region in the case of angled wavy walls (cases 3 and 4) is almost the same as that in the other cases.

Figure 5 shows the mean velocity in the transverse direction as a function of the wall-normal distance. The absolute values of mean velocity increase as the angle decreases. This is due to the secondary flow generated along the ridgelines. The absolute values reach their maxima at 9 wall units from the surface.

Turbulence intensities

Figure 6 depicts the profiles of turbulence intensities. The peak value of turbulence intensity in the streamwise direction decreases with the decrease in the angle. In contrast with this, the values of turbulence intensity in the transverse direction in the buffer region increase with the decrease in the angle. The main flow is accelerated near the uphill region, while it is decelerated near the downhill region. This acceleration and deceleration cause an increase in the streamwise turbulence intensity. This change in the intensity is redistributed to the turbulence intensity in the transverse direction through not only the sustaining mechanism of turbulence but also the secondary flow. Thus, the modification of turbulence intensities is due to the secondary flow.

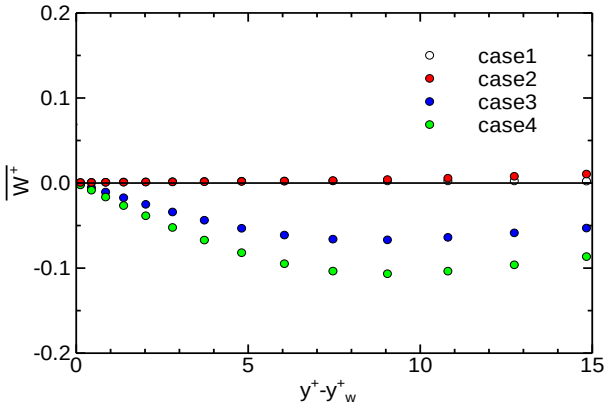

Figure 5. Mean velocity in the transverse direction.

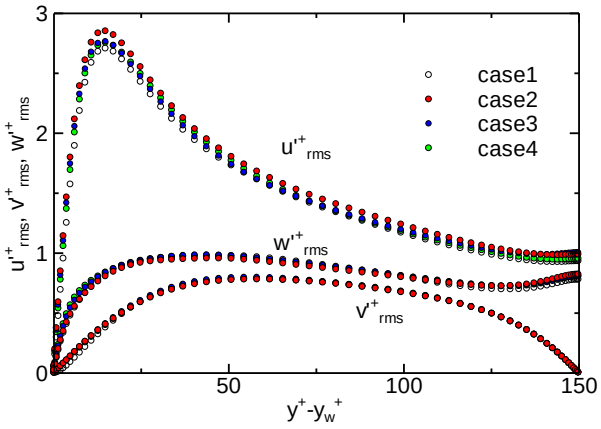

Figure 6. Turbulence intensities.

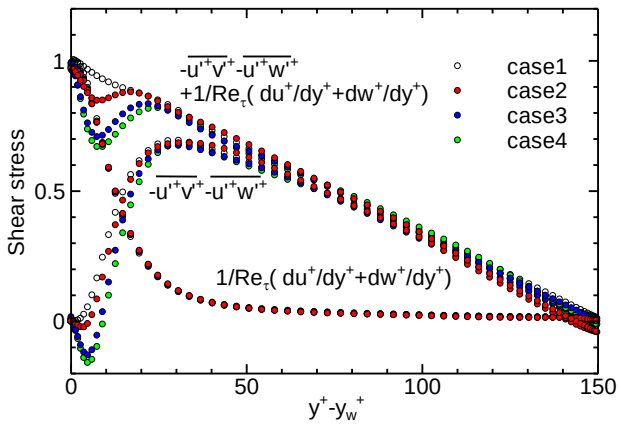

Figure 7. Shear stress tensors.

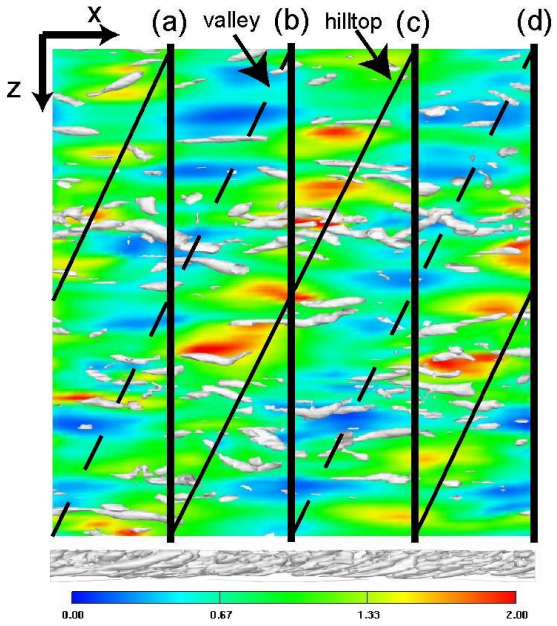

Figure 8. Wall shear stress and vortices (case3).

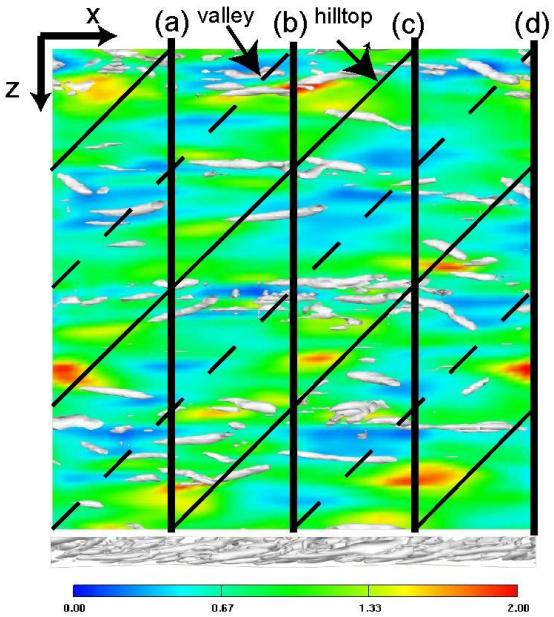

Figure 9. Wall shear stress and vortices (case4).

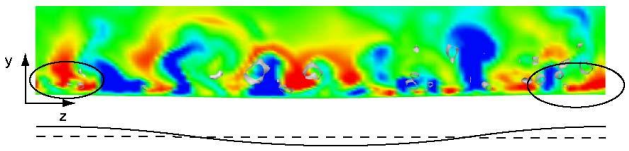

(a) x/h = 1.57

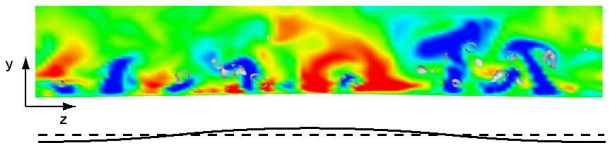

(b) x/h = 3.14

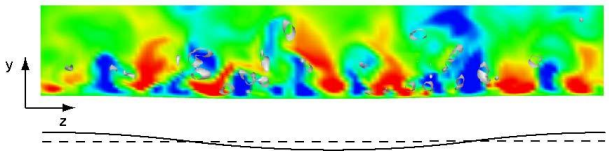

(c) x/h = 4.71

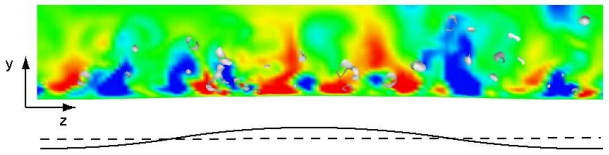

(d) x/h = 6.14

Figure 10. Cross sections of vortices and velocity fluctuations (case3).

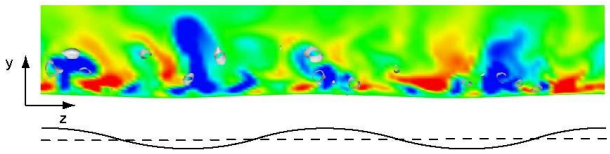

(a) x/h = 1.57

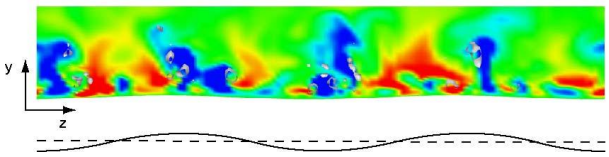

(b) x/h = 3.14

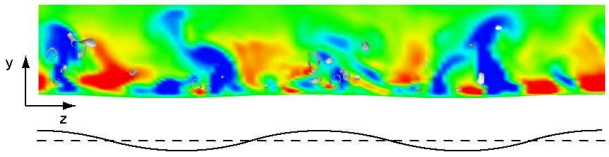

(c) x/h = 4.71

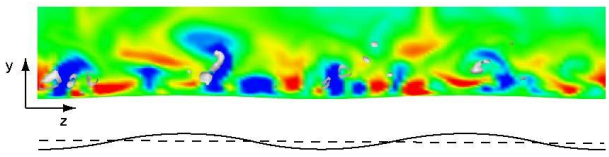

(d) x/h = 6.14

Figure 11. Cross sections of vortices and velocity fluctuations (case4).

Shear stress tensors in flow

Figure 7 indicates the profiles of the averaged shear stress tensor defined by the following equations:

Viscous shear stress: $T = \mu\left(\overline{\frac{\partial u}{\partial y}} + \overline{\frac{\partial w}{\partial y}}\right)$

Reynolds shear stress: $R = -\rho\overline{u'u'} - \rho\overline{u'v'} - \rho\overline{u'w'}$,

where μ and ρ are the viscosity and density. The term $-\rho\overline{u'u'}$ was excluded because this term shows the normal stress. It is found from the figure that the shear stress tensors in the cases of the angled wavy walls are lower than those in the other cases (cases 1 and 2). This is because the contribution of the $-\rho\overline{u'w'}$ component is not negligible due to the secondary flow.

Pressure drag

We examined the values of spatiotemporal average of pressure drag acting on the wavy walls. The pressure drag Dp_x acting on surface element dS is expressed by the following equation:

$$Dp_x = \left(\frac{1}{S}\int_S p\cos\theta dS\right)\cos(\pi - \gamma), \quad (5)$$

where S is the whole surface of the wavy wall. The non-dimensional values of the pressure drag Dp_x^+ was 1.61×10^{-6} in case 2, 2.07×10^{-6} in case 3 and 2.75×10^{-6} in case 4. The dependency of the drag on the angle is consistent with the dependencies mentioned above. However, the pressure drag is much lower than the friction drag because the ratio of the amplitude to wavelength in the present computation is low.

Modification of coherent structure

Figure 8 demonstrates the color contours of wall shear stress and hairpin vortices near the surface in case 3. The identification of vortices is the same as that demonstrated by Jeong and Hussain (1995) and Jeong et al. (1997). The red area indicates higher values of the streamwise component for the wall shear stress tensor, while the blue area indicates lower values of the streamwise component for the wall shear stress tensor. The grey areas show the hairpin vortices. The solid lines and broken lines indicate the ridgelines and the lines connecting the lowest point, respectively. It is found that wall shear stress is locally low near the valleys of the wavy wall, while it is locally high near the hilltops. In case 4, as shown in Fig. 9, the areas of high wall-shear stress become smaller and the areas of low wall-shear stress also become smaller than those in case 3. Consequently, the contour map in case 4 is similar to that in case 1.

To understand the localization of high or low wall shear regions, we examined the flow in the four cross-sectional planes indicated by vertical bold lines in Figs. 8 and 9. Figure 10 illustrates the flow in these four planes in case 3. In this figure, the red area indicates the regions of high-speed streaks, while the blue area indicates the regions of low-speed streaks. The grey areas show the cross-sections of hairpin vortices. In case 3, the hairpin vortices are located far from the valley and close to the hilltop. These vortices are the reason for the change in the Reynolds shear stress shown in Fig. 7. On the other hand, in Fig. 10(a), the low-speed streaks are seen close to the uphill region (i.e. ascending wall) (See the areas inside the ovals). This is due to the fact that the secondary flow interferes with the high-speed streaks coming closer to the wall. On the other hand, in case 4, the low-speed streaks are found even close to the hilltop as shown in Fig. 11. This is different from the streaks in the other cases with the wavy wall. This is due to the fact that the hairpin vortices are attenuated by the secondary flow.

CONCLUSIONS

We have carried out direct numerical simulation for turbulent flow over angled wavy walls. Three different angles between the streamwise direction and the ridgelines of the wavy walls were dealt with. The main conclusions obtained are as follows:

(1) The mean velocity in the transverse direction becomes predominant as the angle decreases. This is due to the occurrence of secondary flow along the ridgelines of the wavy walls.

(2) The wall-shear stress tensor decreases with the decrease in the angle. This is because the contribution of the Reynolds shear stress component $-\rho\overline{u'w'}$ becomes more noticeable as the angle decreases.

(3) The local modification of hairpin vortices and streaks caused by the secondary flow along the ridgelines leads to the decrease in the Reynolds shear stress

REFERENCES

Fish, F. E., 2006, "The myth and reality of Gray 's paradox: implication of dolphin drag reduction for technology", *Journal of Biomim and Bioinsp*. Vol. 1, pp. R17-R25.

Hen, D. S., and Sykes, R. I., 1999, "large-eddy simulation of flow over wavy surfaces", *Journal of Fluid Mech.*, Vol. 383, pp. 75-112

Koyama S., Takashima K. and Hagiwara Y., 2007, "Turbulence Modification in Flow around a Periodically Deforming Film", *J. of Turbulence* Vol. 8, article No. 1, pp. 1-20.

Jeong, J., and Hussain, F., 1995, "On the identification of a vortex", *Journal of Fluid Mechanics*, Vol. 285, pp. 69-94.

Jeong, J., Hussain, F., Schopa, W., and Kim, J., 1997, "Coherent structures near the wall in a turbulentchannel flow", *Journal of Fluid Mechanics*, Vol. 332, pp.185-214.

Nakagawa, S., and Hanratty, T. J., 2003, "Influence of a wavy boundary on turbulence. II. Intermediate roughened and hydraulically smooth surfaces", *Experoments in Fluids*, Vol. 35, pp. 437-447.

Tuan, H., El-Samni, O., Yoon, H. S., Chun, H. H., 2006, "Immersed boundary method for simulating turbulent flow over a wavy channel", *Extended Abstracts of Whither Turbulence Prediction and Control*, pp. 116-117

Yoshitake N., Ozaki Y., and Hagiwara Y., 2008, "Drag acting on small wavy plates on the bottom of an open channel", *Proc. of the 22nd Int. Congress of Theoretical and Applied Mechanics* (CD-ROM), Paper No. 11760, pp. 1-2.

Zhang H., Yoshitake N., and Hagiwara Y., 2007, "Changes in drag acting on an angled wavy silicone-rubber plate as a model of the skin folds of a swimming dolphin", *Bio-mechanisms of Animals in Swimming and Flying*, (N. Kato, S. Kamimura ed.), Chapter 8, pp.91-102, Springer Verlag, Tokyo.